Meteorol. Appl. 13, 179–195 (2006) doi:10.1017/S1350482706002088

A flow regime diagram for forecasting lee waves, rotors and downslope winds

P. F. Sheridan & S. B. Vosper
Met Office, FitzRoy Road, Exeter EX1 3PB, UK
Email: peter.sheridan@metoffice.gov.uk
Submitted 8/3/2005, revised 6/12/2005

The influence of a strong low-level temperature inversion on the occurrence of lee waves, rotors and hydraulic jumps has been investigated using high resolution numerical model simulations. The aim of the work is to develop tools for forecasting hazardous winds downstream of mountains. Two-dimensional simulations were conducted for a range of inversion heights and strengths and a fixed hill shape; lee waves, rotors and hydraulic jumps were found to occur. The flow type depends largely on the ratio of mountain height to inversion height and the upstream Froude number. A flow regime diagram based on these two parameters has been constructed and suggests that rotors could be forecast using upstream profiles, which are generally readily available from numerical weather prediction models.

The applicability of the regime diagram for two-dimensional flow to flows over real terrain has been tested using three-dimensional simulations of flows over East Falkland, South Atlantic, under a range of upstream conditions. The flow type is found to be determined largely by the upstream profiles of wind and temperature, and the maximum height of orography directly upstream, indicating that the flow regime diagram can be used to predict flow type downstream of such terrain. Various three-dimensional flow phenomena occur, such as flow channelling through gaps, and could be taken into account to improve the information available from the regime diagram.

Keywords: flow regime diagrams, non-linear numerical simulations.

Received March 2005, revised December 2005

1. Introduction

The occurrence of severe weather in mountainous regions represents a difficult but important challenge to weather forecasting. Hydraulic jumps, strong downslope winds and turbulent rotors associated with lee waves, are all examples of flow phenomena for which accurate forecasting would improve aviation safety and be of general benefit to populations in mountainous regions. However, current computing constraints mean that damaging gusts occur on scales too small to be resolved by operational numerical weather prediction (NWP) models. Even as these constraints recede, deterministic model forecasts of surface wind are likely to remain problematic due to the chaotic nature of the flow. Thus a forecast of flow *type* may prove more useful.

A number of analytical techniques based on the linear theory for mountain waves are reviewed by Vosper (2003). While these can be used to forecast wave motion based on upstream profiles of wind and temperature, non-linear phenomena such as rotors and hydraulic jumps are not well represented by linear theory. Also, no account is taken of friction at the surface in these methods and hence they cannot be used to provide a forecast of how the waves may affect the near-surface winds. Idealised two-dimensional (2-D) numerical studies of flows over mountains carried out by Doyle & Durran (2002) suggest that the presence of surface friction is crucial to the formation of rotors. They found that for sufficiently large wave amplitudes, the wave-induced pressure field can force boundary-layer separation and recirculation beneath wave crests. Further idealised simulations (Vosper 2004) have begun to examine the atmospheric upstream conditions under which rotors may occur. Vosper's work indicates that lee waves, rotors and hydraulic jumps are likely to occur in the presence of an upstream temperature inversion. The amplitude of the wave response is controlled by the inversion Froude number, F_i, defined in the usual hydraulic way for two-layer shallow-water flow. For sufficiently large wave amplitudes, boundary-layer separation occurs and rotors form. In general, as F_i decreases at a given value of H/z_i, where H and z_i are the mountain and inversion height, respectively, the wave amplitude increases until eventually the lee waves are replaced by a low-level hydraulic jump. These findings were summarised in a flow regime diagram based on the upstream values of F_i and H/z_i. The establishment

of the regime diagram suggests upstream profiles, which are readily available from NWP output, could be used to forecast the flow type downstream of mountain ranges. The main concern in developing the regime diagram as a forecast tool is the extent to which a flow regime diagram based on 2-D flows can be applied to flows in three dimensions over complex orography.

The above issue was investigated by Mobbs et al. (2005) to a certain extent using data from a recent field experiment on the Falkland Islands, South Atlantic. Mount Pleasant Airfield (MPA) is situated to the south of the Mount Wickham range on East Falkland and pilots are frequently warned of 'rotor streaming' in northerly flow. Strong temperature inversions are common in the Falklands during northerly flow, and under these conditions strong downslope winds associated with lee wave activity aloft were observed for extended periods during the experiment. These were often interrupted by short (~1 h) intervals of high spatial variability and unsteadiness in the surface winds, indicative of flow separation and rotor formation. Values of F_i and H/z_i were diagnosed from radiosonde ascents during the experiment. For a given H/z_i, it was found that the periods of flow separation tended only to occur at times when F_i was smaller than some critical value.

In this study the applicability of the regime diagram for 2-D flow to flows over complex three-dimensional (3-D) orography is examined. A set of three very high resolution 3-D simulations has been conducted of northerly flow over East Falkland in which a sharp upstream temperature inversion is present. These simulations will be used to study how the different flow types, which occur in 2-D flow, manifest themselves in three dimensions, and to examine other effects, unique to 3-D flow, which could be relevant for forecasts of hazardous winds. Examples of the latter include splitting of the flow upstream (the flow may pass around rather than over the mountains) and channelling through valleys and gaps in the orography. The 3-D structure of rotors is also likely to be more complex than for 2-D flows and effects such as vortex stretching and tilting may enhance turbulence and give rise to unsteady effects, which are absent in two dimensions. In terms of the practicality of using the regime diagram for forecasting purposes, a key question is 'do the different flow types which occur in 2-D flow occur at the same values of F_i and H/z_i in 3-D flow over complex terrain?' This issue is further complicated by the uncertainty in choosing a representative mountain height, H, in terrain which consists of several mountain peaks. As a first guess one might choose to use the height of the mountain immediately upstream of the area for which a forecast is required. Results from the simulations presented here will be used to assess the extent to which this is true.

As well as presenting results for real terrain, results for idealised 2-D simulations are also presented. These are essentially a repeat of those presented by Vosper (2004), but for a narrower hill. The simulations were carried out to validate a linear theory for lee wave rotors which will be presented in a forthcoming paper, but are included here for the purposes of illustration and to examine the sensitivity of the regime diagram to linear and non-linear forcing.

It should be stressed that since the regime diagram is based on the characteristics of the temperature inversion, a forecast tool developed using the regime diagram would be applicable in the first instance to northerly flows in the Falkland Islands, where strong low-level temperature inversions are the principal source of rotor activity (Mobbs et al. 2005). In the remainder of this paper, Section 2 describes the idealised upstream conditions used. In Section 3, the numerical model is described, and the results of the 2-D and 3-D simulations are presented. Conclusions are drawn in Section 4.

2. Idealised conditions

Following Vosper (2004) an idealised problem was considered wherein the upstream wind speed is constant with height (above the boundary layer). The profile of potential temperature is such that a neutral layer exists in contact with the surface, capped by a sharp temperature inversion, above which the atmosphere is stably stratified with constant Brunt-Väisälä frequency, $N = 0.01\,\mathrm{s}^{-1}$. This profile is shown schematically in Figure 1.

Vosper (2004) found that, while a number of dimensionless parameters control the flow, the principal quantities for the range of conditions under

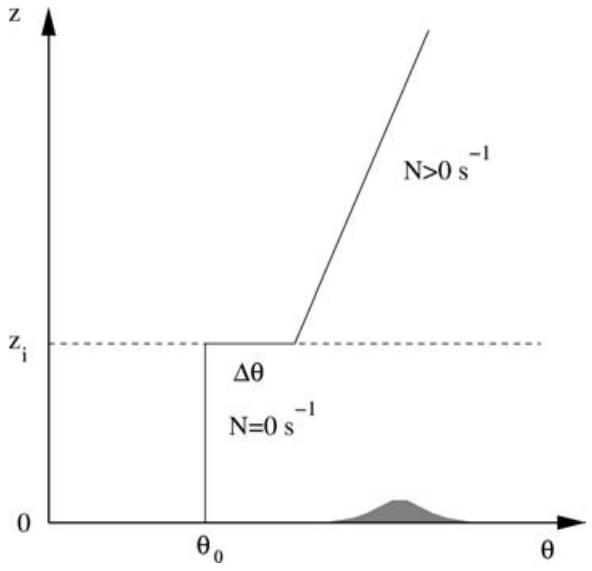

Figure 1. *A schematic diagram illustrating the simple two-layer atmosphere. The inversion, characterised by a discontinuity of magnitude $\Delta\theta$ in the potential temperature, occurs at a height $z = z_i$.*

consideration are:

$$F_i = U/\sqrt{g' z_i}, \quad Z = N z_i / U \quad \text{and} \quad H/z_i, \qquad (1)$$

where U is the upstream geostrophic wind speed, z_i is the height of the inversion, $g' = g\Delta\theta/\theta_0$ is the reduced gravity, θ_0 being the potential temperature in the neutral layer (set to 288.15 K in all simulations), g the acceleration due to gravity and $\Delta\theta$ the difference in potential temperature between the top and bottom of the inversion (inversion strength). The three non-dimensional quantities in (1) are the Froude number, F_i, as defined for shallow water flow (e.g. Baines 1995), the non-dimensional inversion height, Z, and the ratio of the mountain height, H to the inversion height, z_i. According to linear theory, at a given value of Z, there is a critical Froude number above which lee waves cannot exist on the inversion (Vosper 2004). The lee wave wavelength is determined by F_i and Z (see eqn. 15 of Vosper 2004). Meanwhile the amplitude of the waves is proportional to the mountain height and hence H/z_i controls the occurrence of rotors and hydraulic jumps.

3. Numerical simulations

The simulations were performed using the Met Office BLASIUS model (e.g. Wood & Mason 1993), which has been used extensively for a range of orographic flow studies (Wood 1995; Allen & Brown 2002; Vosper 2004). A brief description of the model follows, and further detail can be found in the above references. The general features of the model will be described first, followed by the specific configurations used for 2-D and 3-D simulations.

The model as used here solves the time-dependent Boussinesq equations in a terrain-following coordinate system (Gal-Chen & Somerville 1975) with a first-order mixing length turbulence closure scheme. A no-slip lower boundary condition was applied with a constant roughness length of $z_0 = 0.05$ m. A stretched vertical grid was used to give finer resolution near the ground. The upper boundary of the model was placed at 20 km and a rigid-lid upper boundary condition was applied. The lateral boundary conditions were periodic. A Rayleigh damping layer was placed above 15 km in order to minimise the reflection of upward propagating gravity waves, while Rayleigh damping columns were placed adjacent to all lateral boundaries to prevent wrap-around effects. The temperature inversion is represented by imposing a jump, of size $\Delta\theta$, in potential temperature across a single grid level. The vertical grid spacing over which this was imposed was at most 150 m, and generally less than 100 m. Before the main simulation, a one-dimensional (1-D) solution was first obtained using a 1-D version of the model which was run to a steady state. This resulted in a modification to the wind profile due to turbulent mixing in the layer beneath the inversion while the potential temperature structure was unaltered. Examples of these boundary-layer profiles can be seen in Figure 2 of Vosper (2004). The value of the Rossby number, $R_0 = U/fL \gg 1$ (where f is the Coriolis parameter and L is the mountain width) for all cases here and it seems likely that rotation will have little impact on the dynamics of the flow, other than to modify the upstream wind profile in the boundary layer.

2-D configuration: In 2-D simulations 512 grid points were used in the x (streamwise) direction, with a grid spacing of 125 m. In the vertical, 100 levels were used, the lowest of which was at 10 m. The vertical grid spacing increased smoothly with height from 20 m near the surface to 479 m adjacent to the upper boundary. Using this configuration, repeat simulations of cases in Vosper's (2004) study, where a higher vertical resolution was used, closely reproduced the original results. Rayleigh damping columns of width 8 km were applied at the lateral boundaries. The Coriolis force was imposed with strength $f = 10^{-4}$ s^{-1}. The orography considered was an idealised ridge of the form

$$h(x) = \begin{cases} H\{1 + \cos(Kx)\}/2 & \text{for } |x| \le \pi/K \\ 0 & \text{for } |x| > \pi/K, \end{cases} \qquad (2)$$

where $K = 2\pi/L$ and $x = 0$ is the centre of the model domain. A westerly geostrophic wind was applied, $(U,0)$, where $U = 8$ ms^{-1}. The hill width L was 2.5 km (compared to 10 km in Vosper's (2004) study), and the hill height, H, was fixed at 400 m (as in Vosper's (2004) study). Integration was generally carried out for 30,000 s, by which time transient disturbances generated during the initial stages of the flow evolution had disappeared.

3-D configuration: For the 3-D simulations, 512 grid points were used in the x (east-west) and y (north-south) directions with a uniform grid spacing of 200 m, such that the domain area is 102.4 km × 102.4 km. The vertical grid consisted of 60 levels, the lowest at 10 m. The vertical grid spacing increased smoothly with height from 20 m to 614 m. The lateral Rayleigh damping columns were 3.2 km wide. The Coriolis force was imposed with $f = -1.14 \times 10^{-4}$ s^{-1}, roughly the value at MPA, and a northerly geostrophic wind, $(0,-U)$ was considered, where again $U = 8$ ms^{-1}. The terrain data, obtained from a 100 m resolution digital elevation dataset, are shown in Figure 2. MPA is located roughly in the rectangle shown, whose south-west and north-east coordinates are $(-1,-20)$ and $(4,-18)$ km, respectively. Two distinctive east-west running ridges are present on East Falkland and the longest of these, lying immediately south of its companion, contains orography rising above 600 m in height to the west of $x = 0$ km, with a large area of around 400 m in height to the east of $x = 0$ km. At roughly $x = 0$ km, the ridge height falls to a minimum value of around 140 m.

Simulations were conducted for three upstream inversions. The combinations of inversion height and

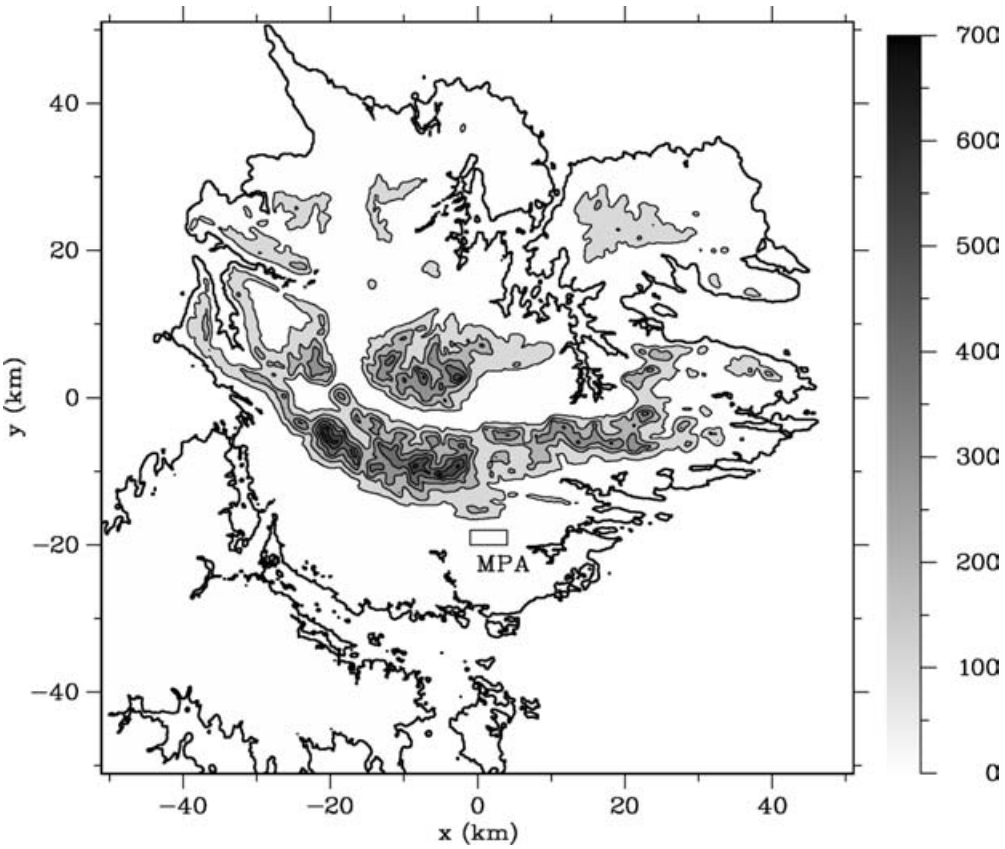

Figure 2. *The orography of East Falkland, South Atlantic. Terrain heights are shown in metres (contour interval 100 m). The location of MPA is marked by the rectangle and the coastline is denoted by the bold contour.*

strength used were $\Delta\theta = 6.53$ K, $z_i = 800$ m; $\Delta\theta = 14.69$ K, $z_i = 800$ m and $\Delta\theta = 5.64$ K, $z_i = 333$ m. This corresponds to $F_i = 0.6$, $U/Nz_i = 1$; $F_i = 0.4$, $U/Nz_i = 1$ and $F_i = 1$, $U/Nz_i = 2.4$, respectively. Note that while the upwind value of Z is unique for a given flow, the varying height of the terrain used means that the appropriate value of H/z_i is less clear. The aforementioned range of terrain heights present within the main ridge corresponds to the range $0.175 < H/z_i < 0.850$ in the first two cases, and $0.42 < H/z_i < 2.04$ in the third case. Integration was carried out for roughly 14,000 s and the character of the flows was well established by about 10,000 s.

3.1. Two dimensional flows and the regime diagram

A range of 2-D simulations was carried out, essentially repeating those of Vosper (2004) with a narrower mountain. As explained by Vosper (2004), using a mountain width of 2.5 km (as described earlier in this section) results in the wave forcing being primarily linear, whereas for the 10-km wide mountain used in Vosper's original simulations, the wave amplitude was controlled by non-linear processes. A range of inversion strengths, $\Delta\theta$, and inversion heights, z_i, were used, such that $0.2 \leq F_i \leq 1.2$ and $0.125 \leq H/z_i \leq 1$. Note that the values of U, N and H used mean that $Z^{-1} = 2H/z_i$. Figures 3a and 3b show the resulting flows after 30,000 s (by which time the flows had been steady for at least 6000 s) when $F_i = 0.6$, $H/z_i = 0.5$ and $F_i = 0.4$, $H/z_i = 0.5$, respectively.

In Figure 3a a lee wave occurs, accompanied by rotors which recirculate beneath the wave crests (as evidenced by the reversed near-surface flow), while the flow shown in Figure 3b contains a hydraulic jump. Both flows present hazards to aircraft flying downstream of the orography. Strong near-surface downslope winds are present in both simulations and, in the hydraulic-jump case, these winds extend far downwind of the mountain. Flow separation occurs in Figure 3a at the upstream edge of each rotor, implying that in reality boundary-layer turbulence would be transported away from the surface to higher levels within the boundary layer. Meanwhile, in Figure 3b the flow is characterised by very strong updraughts immediately downwind of the initial downslope flow, overturning isentropes and an elevated turbulent region (above the boundary layer) which extends downwind of the jump. These flows are very similar to those described by Vosper (2004) for the same upwind parameters and hill height. The flows in all of the 2-D simulations conducted are summarised in a flow regime diagram in Figure 4. In general, as F_i increases at a given H/z_i, the lee wave amplitude decreases until, above a critical Froude number, no lee wave is discernible in the flow. As F_i decreases,

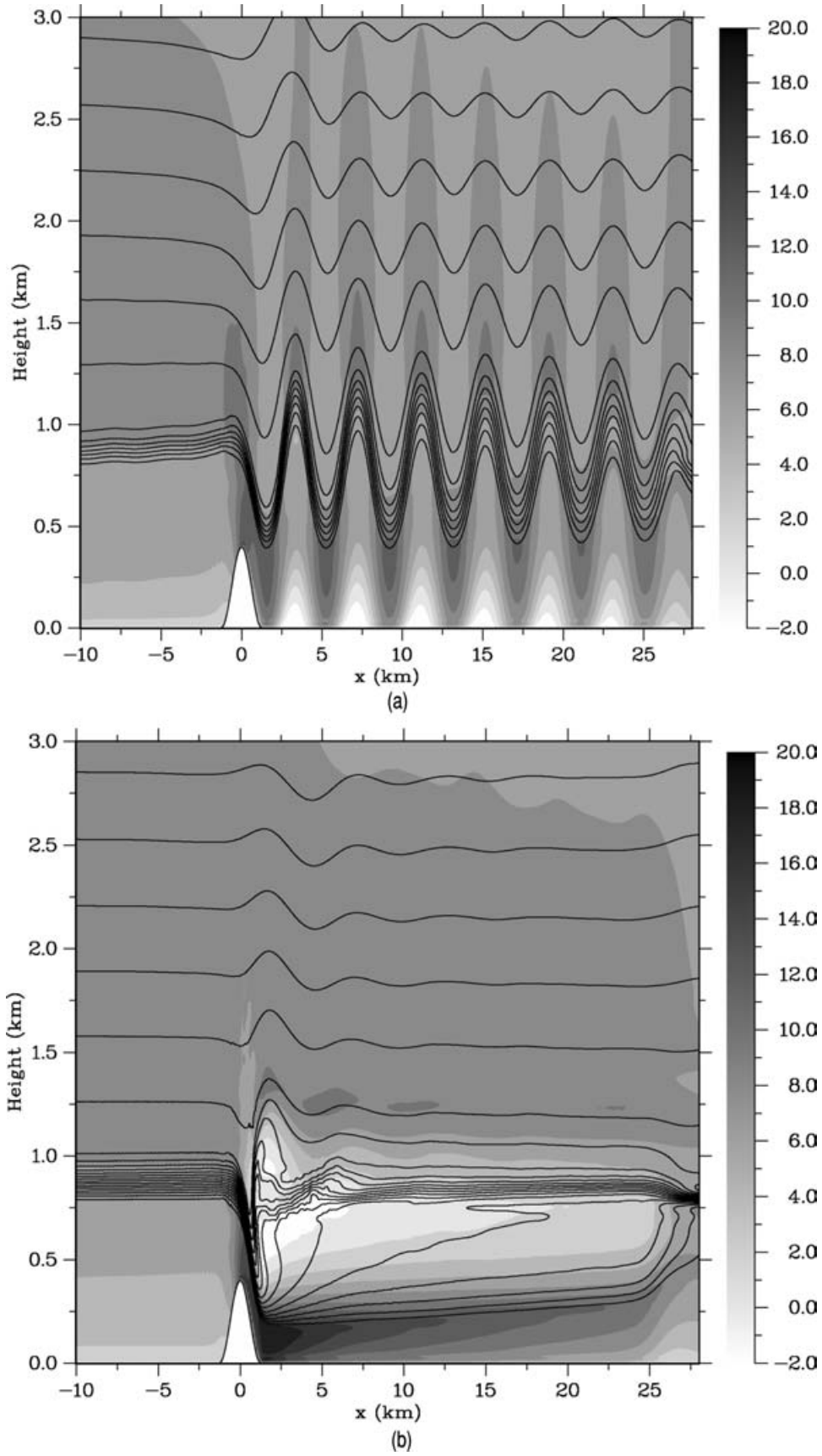

Figure 3. *The flow fields in 2-D simulations after an integration time of 30,000 s when (a) $F_i = 0.6$, $H/z_i = 0.5$, corresponding to an inversion height and strength of $z_i = 800$ m, $\Delta\theta = 6.53$ K; (b) $F_i = 0.4$, $H/z_i = 0.5$ ($z_i = 800$ m, $\Delta\theta = 14.69$ K). Quantities shown are the x velocity component (shaded contours, units ms^{-1}) and potential temperature (line contours, interval = 1 K). In each panel, flow is from left to right.*

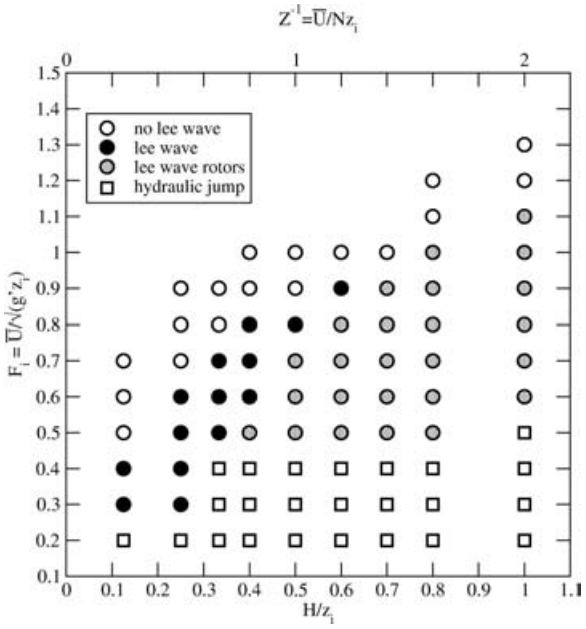

Figure 4. *A flow regime diagram showing the F_i and H/z_i dependence of the flow in the 2-D simulations.*

the lee waves are eventually replaced by a hydraulic jump. Figure 4 and Vosper's (2004) Figure 9 appear very similar, and the reduction in hill width, despite changing the nature of the wave forcing, has only a small effect upon the regime diagram.

3.2. Applying the regime diagram to three-dimensional flow

$$F_i = 0.6,\ U/Nz_i = 1 \tag{1}$$

Three simulations of flow over East Falkland were performed using upstream profiles where $F_i = 0.6$, $U/Nz_i = 1$; $F_i = 0.4$, $U/Nz_i = 1$; and $F_i = 1$, $U/Nz_i = 2.4$. Note that $Z^{-1} = U/Nz_i$ has been used to specify the inversion height since this is unique and independent of the orography. Animations illustrating the temporal evolution of these flows are to be presented in a further paper in electronic form (Sheridan & Vosper 2005).

Figure 5a shows a horizontal slice of the vertical velocity field at a height of 1000 m when $F_i = 0.6$ and $U/Nz_i = 1$ after 10,000 s of integration. Downstream of the ridge a lee wave field is visible as a series of parallel bands of strong up- and down-draughts in which the maximum vertical speeds reach around 4 ms^{-1}. Figure 5b shows the cross-ridge southerly wind component at 10 m above the surface reflects the wave pattern above, where the surface winds are perturbed by the lee wave pressure field. Regions enclosed by a dotted line indicate where flow reversal occurs (i.e. where the flow has a southerly component). The extensive lee wave signature is absent downwind of the highest orography located between $x = -21$ km and $x = 0$ km. Instead, at the surface, a very different pattern of regions of high and low wind, orientated roughly perpendicular to the ridge occurs. The slack areas extend far downstream and are clearly not associated with lee waves. The two bold lines in Figure 5b indicate vertical cross sections through the flow field that will be discussed in the following text. One of these slices passes through the west part of the range, where the orography is relatively high, and the streamwise flow must pass over two ridges. The other slice passes through the east part of the range, where a single ridge occurs, which is significantly lower than the orography to the west.

The flow downstream of the eastern half of the ridge and across MPA is examined first, and then the non-lee wave flow downstream of the west portion of the ridge. A vertical cross-section through the eastern half of the ridge at $x = 13.7$ km, showing wind and potential temperature contours is presented in Figure 6a (position indicated by the right of the two bold straight lines in Figure 5b). The lee waves are regular and propagate far downstream of the mountains. Rotors occur beneath the wave crests, indicated by reversed flow at the surface beneath streamwise flow aloft. The rotor position, shape and intensity were found to fluctuate over time. Figure 7a shows the flow at 10 m downstream of the eastern half of the ridge in close-up. The bands of slack and accelerated flow are not uniform, containing small-scale fluctuations in the surface wind along their length, such as the eddies of size approaching the grid scale ($\sim$400 m) around (15,$-$12.5) km and (19,$-$12.5) km. Over time, the bands remain stationary, but the surface wind fluctuations propagate towards the west, with an apparent speed of $\sim$2 ms^{-1}, comparable to the typical easterly wind component magnitude at 10 m. Clearly, the lines along which flow separation and reattachment occur in the rotor are highly irregular and unsteady. This, combined with the unsteadiness of the cross-section presented in Figure 6a at subsequent times indicates that the rotor has a complex and evolving 3-D structure. The relative uniformity in height of the ridge in this area suggests that an upstream H value of roughly 400 m can be assumed with some confidence here. It is encouraging that the waves in Figure 6a closely resemble in wavelength and amplitude those in Figure 3a resulting from the 2-D simulation carried out under the same conditions. The waves in Figure 6a appear to decay in strength downstream, but inspection of Figure 5a shows that the waves in fact retain their overall amplitude. The wave field does, however, contain areas where wave activity is weaker, presumably due to interference between waves originating from neighbouring points in the orography. The wave field across MPA is similar to that downstream of the eastern part of the ridge. Winds at the surface, however, are higher; flow reversal and rotors are less intense and surface wind speed maxima are greater than those downstream of the eastern half of the ridge. The regime diagram in Figure 4 indicates that rotors become less likely at a given F_i as H/z_i decreases. The low orography upstream of MPA relative to that

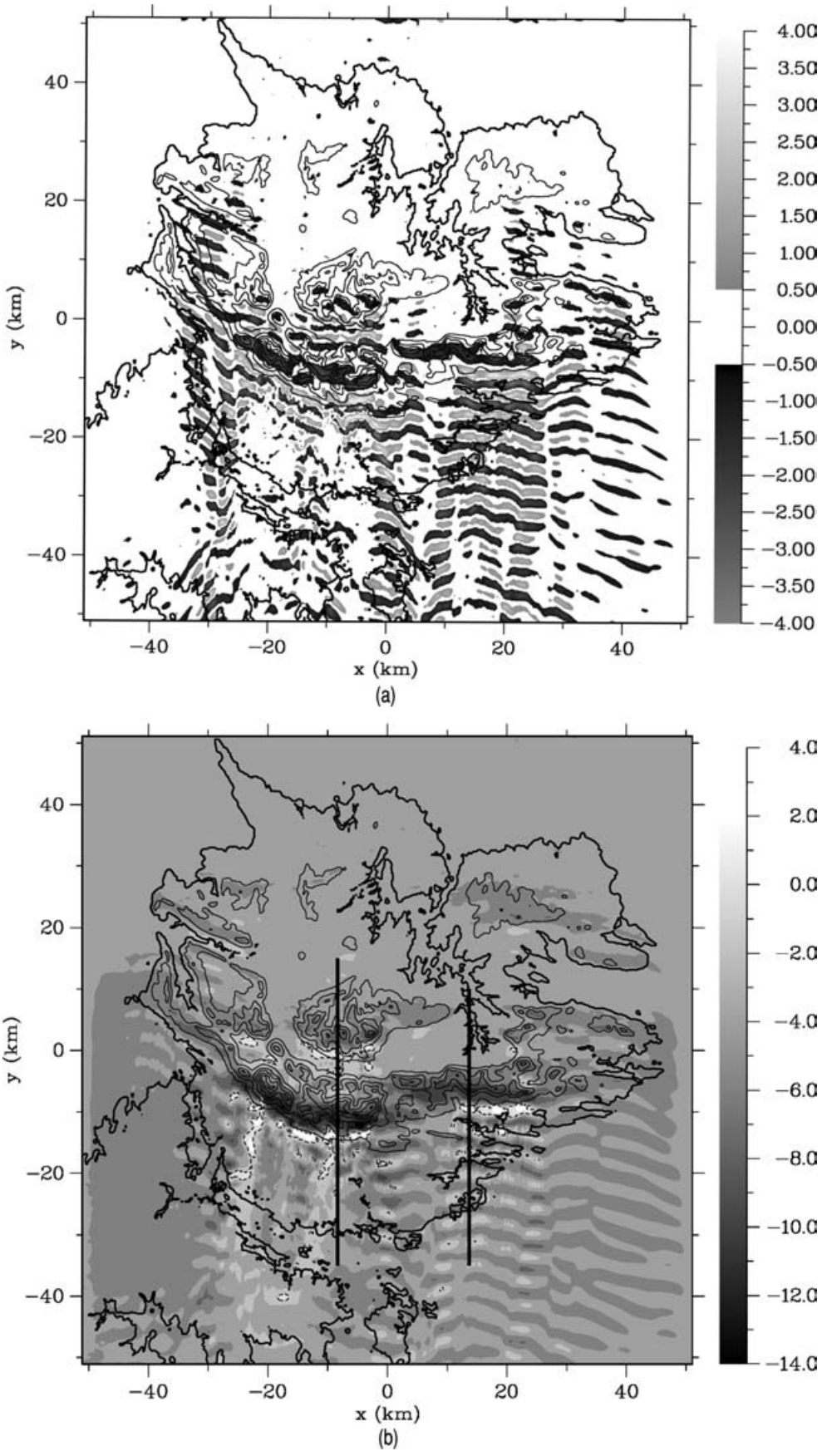

Figure 5. *The 3-D simulated flow field when $F_i = 0.6$, $U/Nz_i = 1$, after 10,000 s of integration time. Quantities shown are (a) vertical velocity at 1000 m (shaded contours, units ms^{-1}) and (b) the southerly velocity component, v, at 10 m (shaded contours, units ms^{-1}). Note that in (a) values between −0.5 and 0.5 ms^{-1} have not been shaded for the sake of clarity and that in (b) the dotted line indicates where $v = 0$ ms^{-1}. Terrain contours are shown in both (a) and (b) with an interval of 100 m. The bold straight lines indicate the positions of vertical cross sections discussed in the text.*

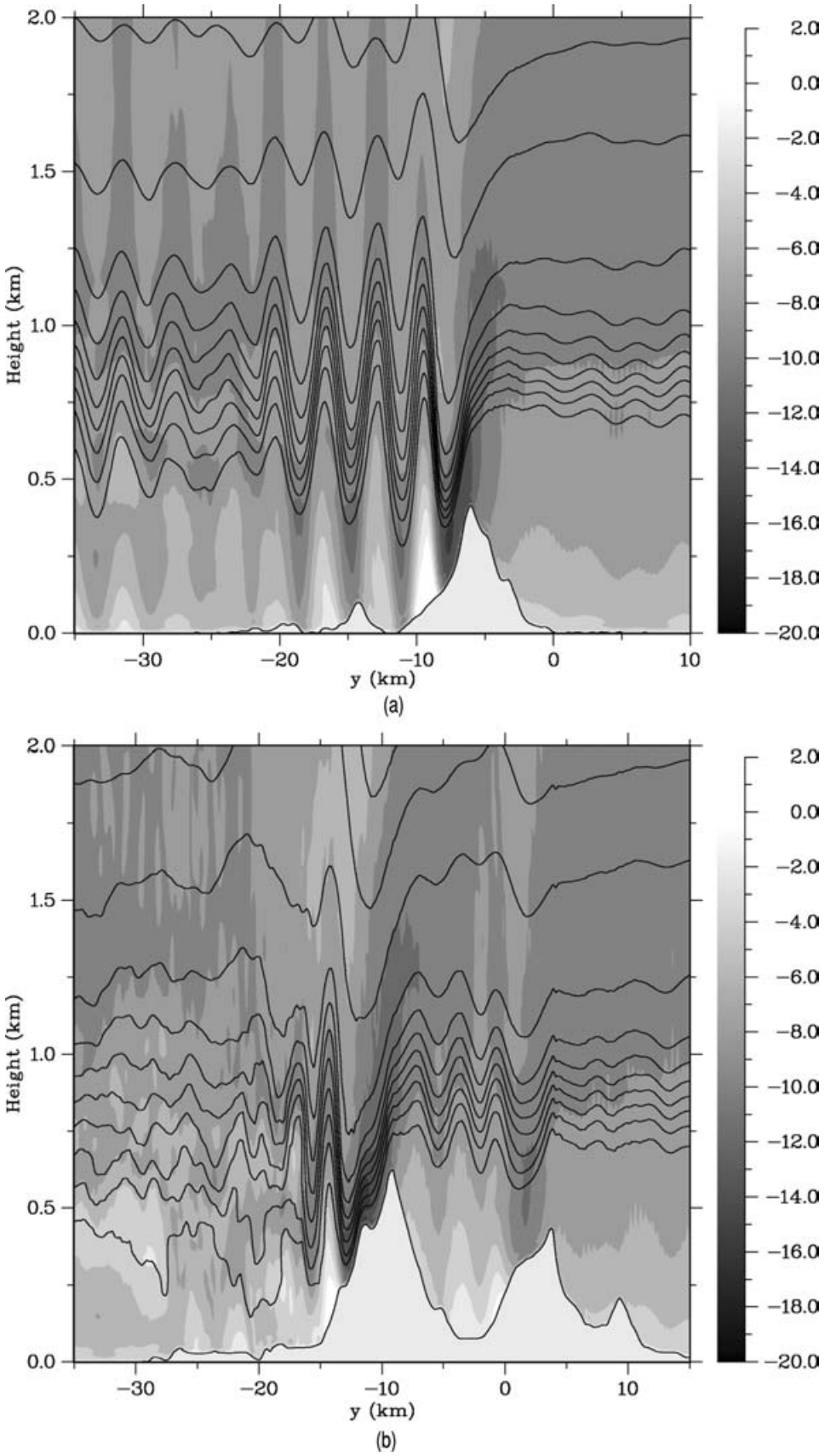

Figure 6. *(a) A vertical north-south cross-section through the flow field at x = 13.7 km showing the southerly wind component (shaded contours, units ms^{-1}) and potential temperature (line contours, spacing 1 K) after 10,000 s of integration. Results are shown for the 3-D $F_i = 0.6$, $U/Nz_i = 1$ simulation. Figure (b) is as for (a) but at x = −8.3 km, after 11,200 s of integration. In each panel, flow is from right (north) to left (south).*

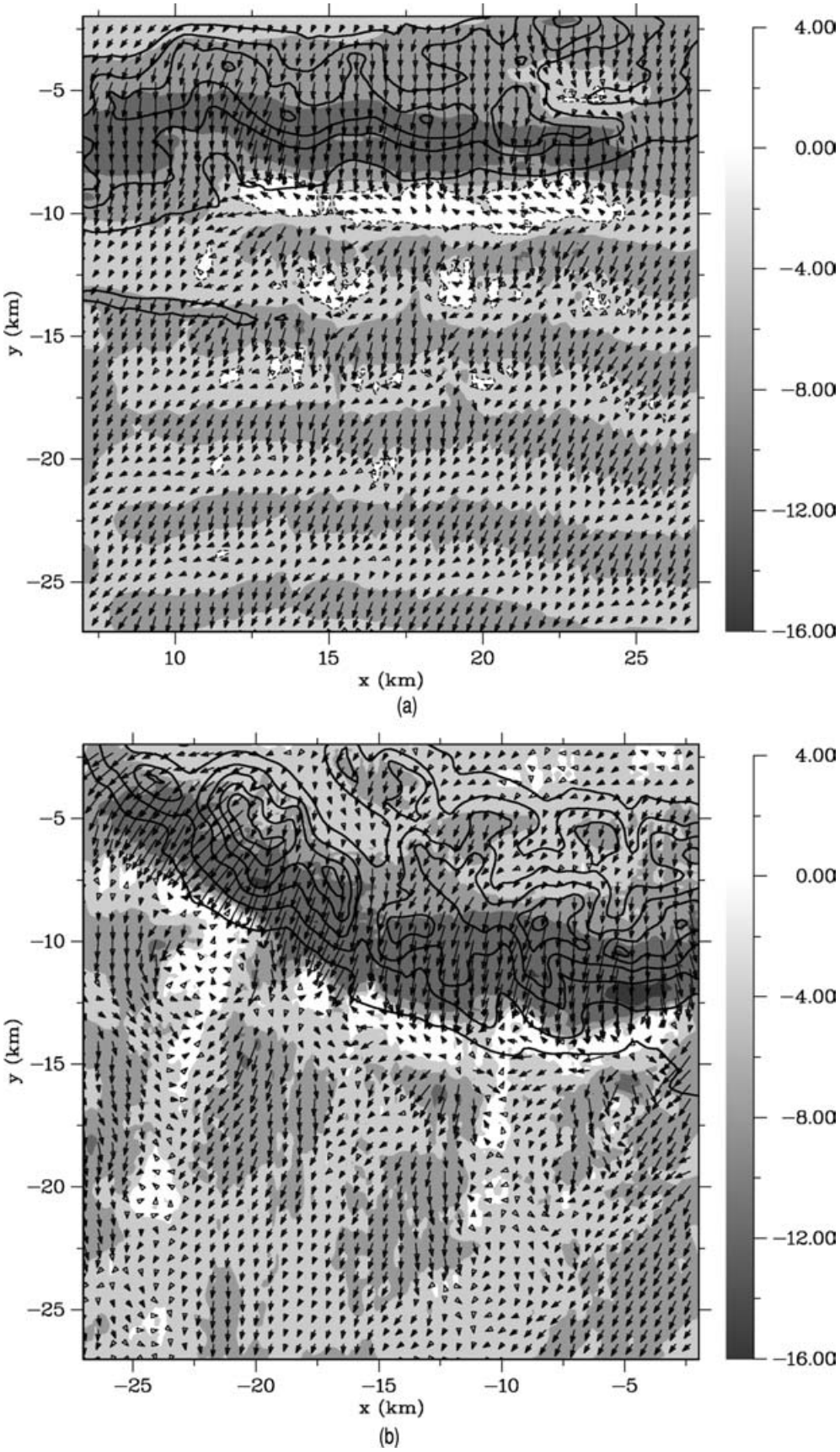

Figure 7. *(a) 10 m horizontal winds in the 3-D $F_i = 0.6$, $U/Nz_i = 1$ simulation after 10,000 s of integration time. Quantities shown are wind vectors and the southerly flow component, v, (shaded contours, units ms^{-1}). A dotted line indicates where $v = 0\ ms^{-1}$. Also shown are the terrain height contours (interval 100 m). Results are shown for a region downstream of the eastern part of the Wickham range. Figure (b) is as for (a) but for the western half of the Wickham range, after 11,200 s of integration.*

to the east is consistent with the appearance of weaker rotor activity if the value of H is taken as that directly upstream. Channelling through the broad gap to the north of MPA may also accelerate the surface winds. This may in addition increase the effective Froude number over the peak at (0,−15) km (named 'Pleasant Peak') and according to Figure 4, further decrease the likelihood of rotor formation.

Figure 6b shows a vertical cross section of the flow at $x = -8.3$ km, in the western portion of the ridge (position indicated by the left of the two bold straight lines in Figure 5b). The flow is hydraulic jump-like; the coherent wave train evident further east (Figure 6a) is absent, and the flow undergoes a jump in a transition to a turbulent region downstream. Flow separation occurs at the jump and this results in strong recirculation in the near-surface flow downstream. This part of the ridge frequently rises well above 400 m in height suggesting a higher value of H than for the eastern portion of the ridge is appropriate. The regime diagram, Figure 4, indicates hydraulic jumps become more likely as H and hence H/z_i increase. Note, however, that according to Figure 4, a Froude number of 0.5 or less is required for hydraulic jump formation. One simple explanation for this is that the flow across the southern-most ridge may have already been significantly modified by the orography further north. Indeed, wave motion, with associated rotors (denoted by the flow reversal) is clearly present in Figure 6b above the valley between the two ridges. It seems likely that there has been sufficient modification to the flow to cause a somewhat different behaviour downwind of the southern ridge from that expected for an undisturbed 2-D flow across an isolated ridge. The surface flow downstream of the western half of the ridge at 11,200 s is depicted in close-up in Figure 7b. The elongated region of reversed flow parallel to and at the foot of the ridge is associated with the rotor recirculation described above. The alternating bands of slack flow and accelerated flow which are oriented approximately north-south in this region are wakes and channelled flows originating from isolated peaks and gaps in the upstream orography. The slight westward offset in orientation of these bands is consistent with the turning of the wind at low levels in the boundary layer. The wakes exhibit a great deal of unsteadiness and large eddies are shed downstream of the highest point in the range at around $x = -22$ km (a pair of counter-rotating eddies are visible in Figure 7b at around $y = -11.5$ km). Fluctuations in the position, shape and intensity of the reversed flow regions are also greater than under the lee wave field to the east.

$$F_i = 0.4, \;\; U/Nz_i = 1 \qquad (2)$$

The vertical velocity field at 1000 m after 10,000 s of integration when $F_i = 0.4$ and $U/Nz_i = 1$ is shown in Figure 8a. At this Froude number lee wave trains occur downstream of orography up to around 300 m in height, i.e. where $H/z_i \leq 0.325$. The vertical velocities associated with the waves have magnitudes less than 3 ms^{-1}. Cross sections of the flow at $x = 13.7$ km and $x = -5.1$ km are shown in Figures 9a and 9b respectively (positions indicated by the right and left bold lines in Figure 8b respectively). These demonstrate that where the upstream orography is above 300 m, so that $H/z_i > 0.325$, a hydraulic jump flow now occurs. This transition from lee waves to a hydraulic jump depending on H/z_i is consistent with the regime diagram, Figure 4, when $F_i = 0.4$. Figure 8b shows the 10 m winds and the southerly velocity component. Alternating bands, oriented downwind, of slack or reversed flow and accelerated flow occur downstream of the western half of the ridge, as seen at $F_i = 0.6$, only now more intense. The gap flows between $x = -20$ km and $x = -10$ km are of sufficient strength to prevent the occurrence of an extensive rotor at the foot of the mountain. The hydraulic jump flow that now occurs downstream of the eastern half of the ridge in Figure 8b contains the alternating bands of slack or reversed flow and accelerated flow associated with isolated peaks and gaps, but again no elongated rotor structure is present.

Some of the highest surface wind speeds in the simulation occur in flows associated with gaps or fall-off in the ridge profile. These flows interfere with adjacent lee wave fields. For instance, at around $x = 0$ km (over MPA) and $x = -30$ km, the surface wind is much greater than can be explained by the presence of the lee waves alone. The combination of the velocity perturbations due to the lee wave field and acceleration and unsteadiness of the gap flow serves to create a region of strong winds that are highly variable both spatially and temporally.

$$F_i = 1, \;\; U/Nz_i = 2.4 \qquad (3)$$

This case involves an inversion at a height of 333 m, below the height of much of the terrain. Flows containing such low level inversions were frequently observed during the recent field campaign on East Falkland (Mobbs et al. 2005). This situation is not marked on the regime diagram since, when the upstream inversion lies significantly below the mountain top height, preferential flow around the ridge becomes likely and results obtained using an infinite 2-D ridge may be called into question. The flow is therefore more amenable to study in three dimensions.

Figure 10a shows the vertical velocity field at 400 m for this simulation after 10,000 s of integration. The image suggests that lee waves may be occurring downstream of the majority of the orography, but seem to decay with distance downstream from the ridge. Figures 11a and 11b show vertical cross-sections of the flow at $x = 13.7$ km and $x = -16.9$ km respectively (positions indicated by the right and left bold lines in Figure 10b respectively). Immediately downstream of both regions of the ridge a hydraulic jump-like flow is in fact present, with lee waves downstream of the jump in Figure 11a. The 10 m winds shown in Figure 10b contain the

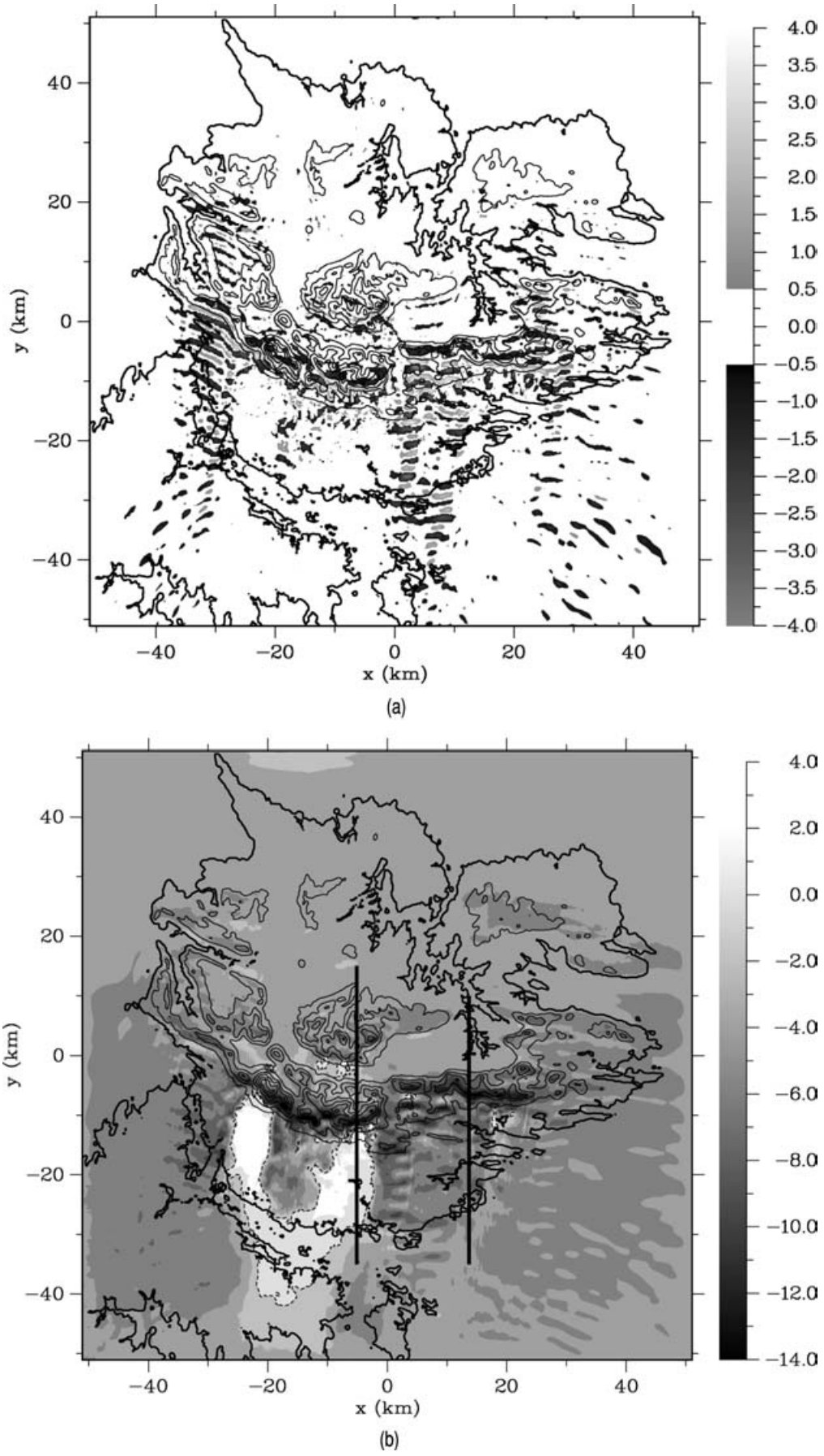

Figure 8. *As for Figure 5, but for* $F_i = 0.4$, $U/Nz_i = 1$.

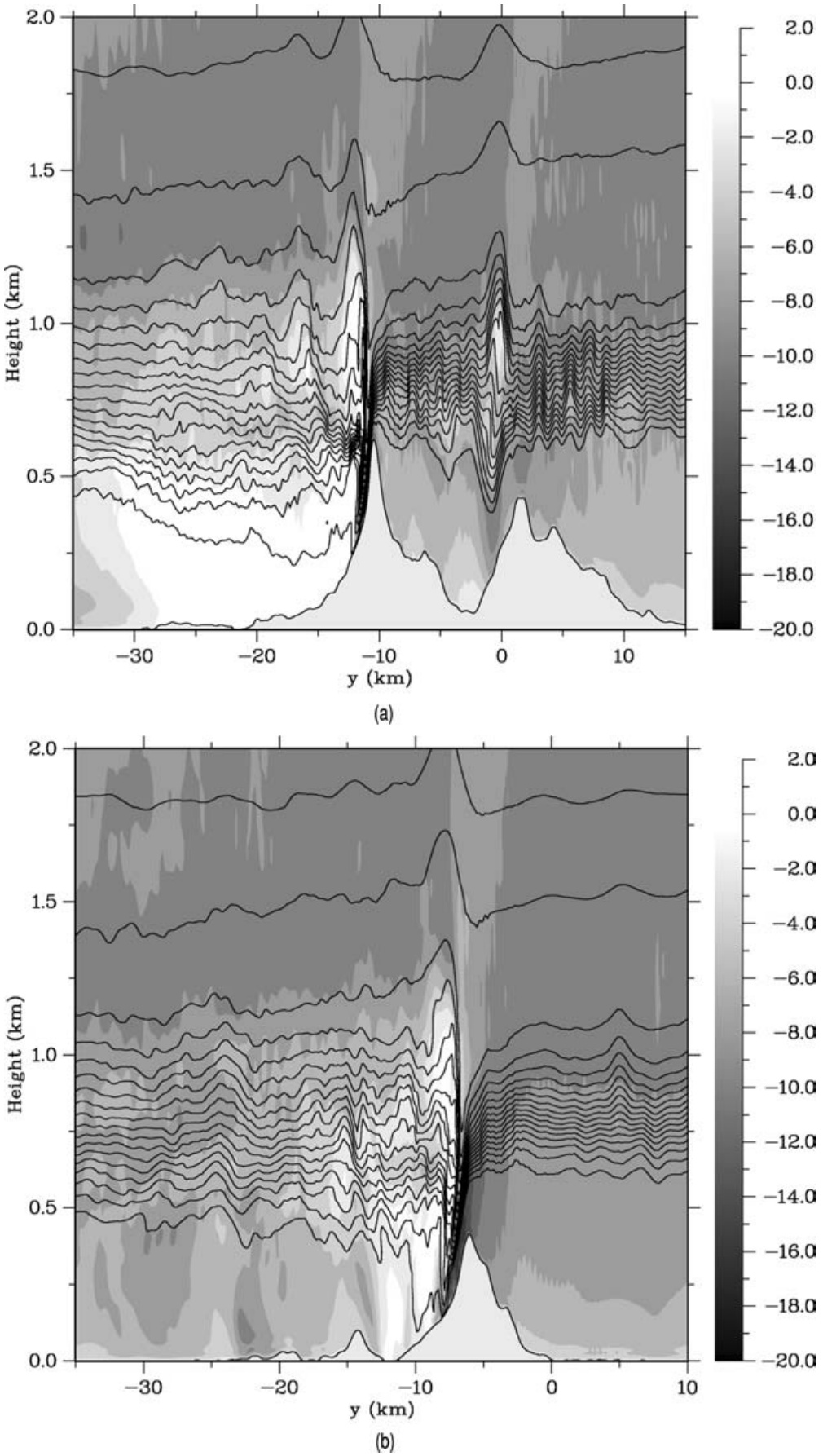

Figure 9. *As for Figure 6 but for the $F_i = 0.4$, $U/Nz_i = 1$ simulation (a) at $x = -5.1$ km after 10,000 s of integration, and (b) at $x = 13.7$ km after 10,000 s of integration.*

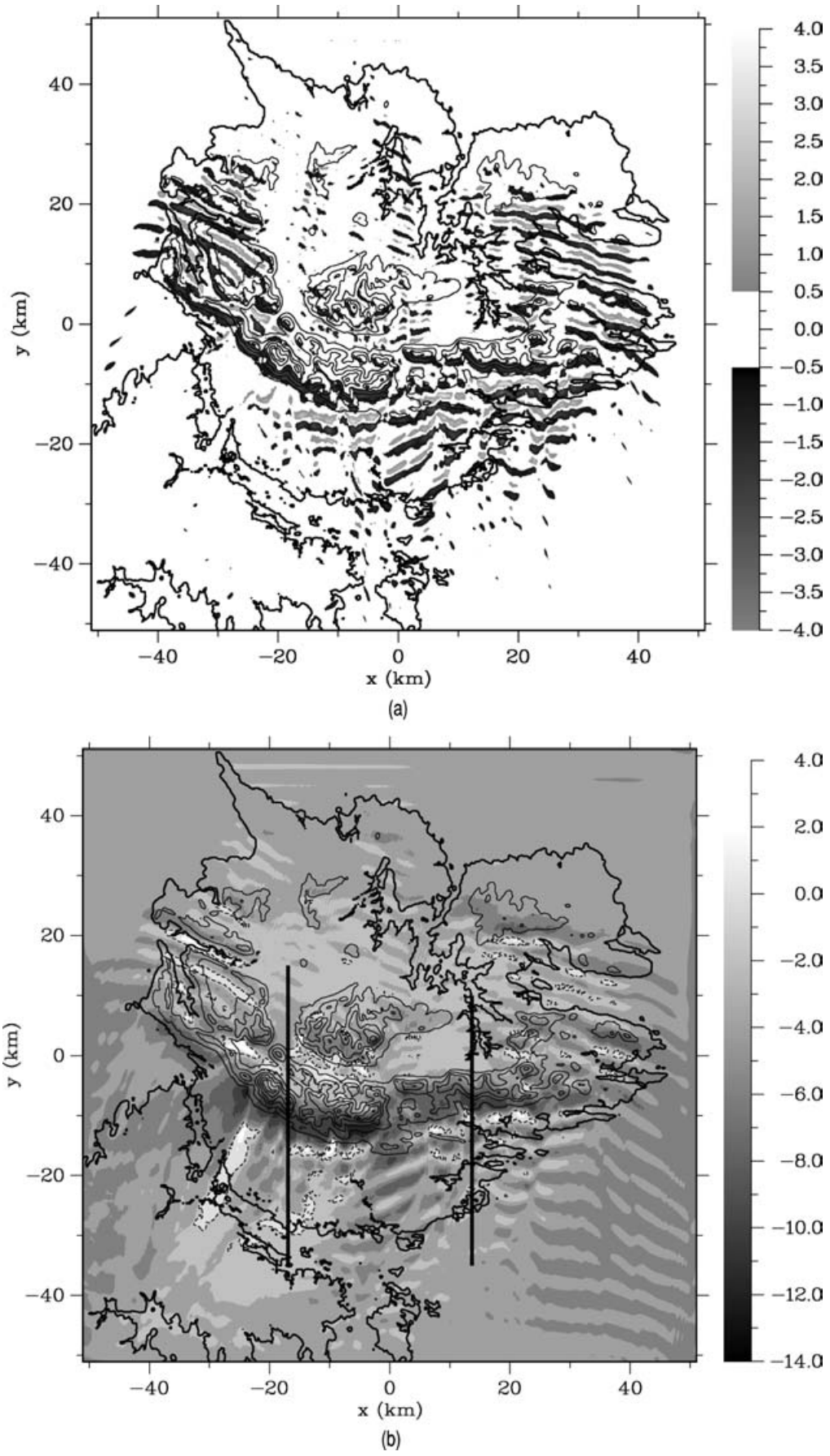

Figure 10. *As for Figure 5, but for the $F_i = 1$, $U/Nz_i = 2.4$ 3-D simulation.*

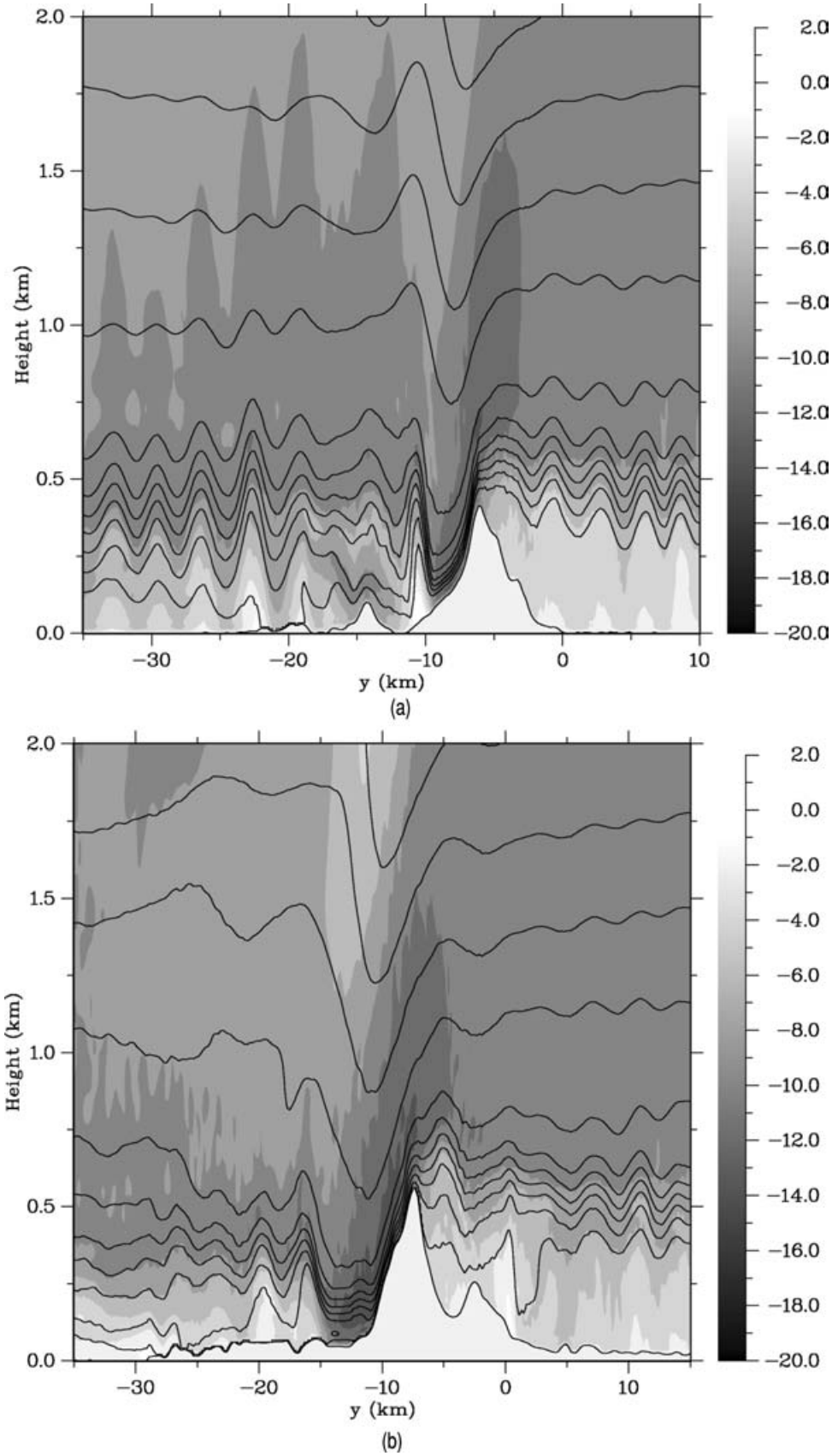

Figure 11. *As Figure 9, but for the $F_i = 1$, $U/Nz_i = 2.4$ 3-D simulation at (a) $x = 13.7$ km, and (b) at $x = -16.9$ km.*

influence of these lee waves, and wakes similar to those in case (a) ($F_i = 0.6$, $U/Nz_i = 1$) can be seen downstream of the western half of the ridge. Given the results summarised in the regime diagram for 2-D flows, a hydraulic jump at such a high upstream Froude number is perhaps unexpected. The following factors may be

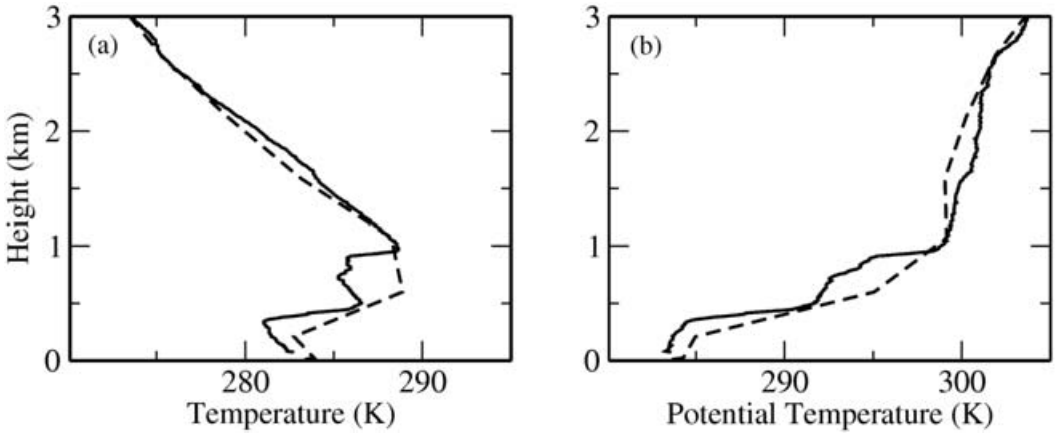

Figure 12. *Comparison of profiles of (a) absolute temperature and (b) potential temperature obtained from a radiosonde launch at 0500 UTC on 9 April 2001 (solid) and from the Met Office global model forecast valid for 0600 UTC on 9 April 2001 (dashed).*

suggested as possible causes of the jump. An increased amount of blocking occurs in this simulation, resulting in a lower upstream wind speed (compare Figure 10b with Figure 8b, and Figure 11a with Figure 9b). This implies a decrease in the effective upstream Froude number. Also, the proximity of the inversion to the mountain-top height is expected to increase the non-linearity of the flow. Both factors make a hydraulic jump more likely. Another feature of this simulation is the relatively shallow boundary layer, in which pronounced wind turning leads to a more northeasterly direction in the trailing of the wakes at the surface in Figure 10b.

4. Discussion and conclusions

A regime diagram has been developed for lee waves, rotors and hydraulic jumps in two-dimensional flows in the presence of a sharp upstream temperature inversion. The regime diagram indicates that the flow type depends largely on the upstream value of the Froude number (F_i) and the ratio of mountain height to inversion height (H/z_i). This suggests upstream profiles, which are readily available from NWP output, could be used to forecast the flow type downstream of mountain ranges. For this to be possible, the regime diagram must be applicable to flows over complex three-dimensional orography. This has been investigated using very high resolution three-dimensional numerical simulations of flows over East Falkland, South Atlantic. The flow type which occurs is generally consistent with the regime diagram, based on the value of F_i and taking H/z_i to be defined with respect to the highest orographic peak directly upstream. This indicates that the regime diagram could be used to predict the flow type downstream of such terrain.

Clearly, the usefulness of a regime diagram approach for forecasting rotors depends to a large extent on the accuracy of the NWP forecast profiles of wind and temperature, upon which the values of F_i and H/z_i are based. The year-long time series of surface wind observations for MPA obtained by Mobbs et al. (2005) have been examined and a list of northerly flow periods during which rotor activity was evident, compiled. Such periods constitute roughly half the number of episodes of northerly flow observed between November 2000 and October 2001. This list of rotor cases was then compared to values of F_i and U/Nz_i computed from the upwind profiles of wind and temperature forecast by the global Met Office Unified Model at 3-hour intervals. Whilst a large proportion (86%) of the NWP forecast profiles contained inversions during the periods when rotors were observed at MPA, the values of F_i and U/Nz_i diagnosed from the profiles suggested that lee waves would be supported (as predicted by Vosper's (2004) linear theory critical value of F_i) for only a small fraction (19%) of the observed rotor cases. This under-prediction is presumably connected with inadequate vertical resolution in the forecast model and the typically sharp nature of the inversions experienced over the Falkland Islands, resulting in under-prediction of the inversion strength and thus over-prediction of the Froude number. For periods when rotors were not observed at MPA, 49% of the corresponding forecast profiles contained inversions, though only 5% yielded values of F_i below the critical value required for lee wave formation, suggesting that the regime diagram technique would rarely provide a false warning of rotor activity.

An example of the forecast profiles is presented in Figure 12, which shows a comparison between forecast and observed profiles of temperature and potential temperature at MPA. The radiosonde was released at 0500 UTC on 9 April 2001 and the forecast profile (taken from a 6-hour forecast) is valid at 0600 UTC on the same day. Whilst the broad structure of the temperature profile is well represented, the structure of the inversion near the surface is necessarily simplified. The strength ($\Delta\theta$) of the forecast inversion is around

10 K compared to roughly 15 K in the measured profile. This under-prediction of the inversion strength suggests that some re-tuning of the regime diagram to allow for the effects of inadequate resolution might substantially improve its success in forecasting rotors. Indeed, the Froude number diagnosed from the forecast profiles was found to be below 2 for 66% of the observed rotor cases at MPA, indicating that there may be some scope for adjusting the values of F_i and H/z_i which delineate the transition from one flow type to another.

Overall the above analysis suggests that the regime diagram is likely to be a useful forecasting tool for the Falkland Islands, although trialling with an up-to-date NWP model is clearly desirable. The method is of course only applicable to regions where strong temperature inversions are common; according to the study by Mobbs et al. (2005) strong inversions ($\Delta\theta >$ 5 K) in northerly flow are observed at MPA roughly 40% of the time. In other regions, where strong temperature inversions are largely absent and lee waves are controlled by the variation of wind and stability over the depth of the troposphere, application of the current regime diagram technique may not be appropriate.

In certain circumstances, the simulations indicate that the flow type in three dimensions may differ from that predicted by the regime diagram for 2-D flows. For example, in highly complex orography the flow over a peak may be perturbed by other terrain features further upstream. In some cases the effect of this might simply be to alter the effective values of F_i and H/z_i from the upstream values, in which case the regime diagram might still be applicable with suitable adjustment of these parameters. However, in cases where upwind lee waves or rotors are present, the influence on the final downstream flow is uncertain. In one of the simulated cases, this resulted in a hydraulic jump occurring at an upstream Froude number just outside the range where such a jump would be expected. The orography of East Falkland, whilst complex, is relatively isolated, with limited scope for interactions between flows from different peaks. Further study of the effect of increasing orographic complexity on the accuracy of the regime diagram will therefore be useful for application of the regime diagram to other locations.

When flow of a given type is established, three-dimensional phenomena which accompany the flow type can significantly affect the surface winds. For instance, hydraulic jump flows are accompanied in the 3-D simulations by wakes from isolated peaks, and gap flows. These decelerate or accelerate, respectively, the flow near the surface for a long distance downstream (typically more than 10 km). The intensity of the acceleration (deceleration) associated with gap flows (wakes) depends on the presence and dimensions of gaps (isolated peaks) in the orography at a given F_i. In addition, these features are more severe for the smaller of the F_i values considered (when the upstream inversion is located at a height above the mountain top height). A sufficiently strong gap flow is able to prevent an extensive rotor from forming downstream of a hydraulic jump. The trailing direction of the wakes and gap flows depends on the wind direction, or more generally the variation of the wind direction with height, at low levels.

In contrast to 2-D simulations which progress to a steady state, the 3-D simulations display temporal unsteadiness. High degrees of unsteadiness are typically observed during rotor episodes (Mobbs et al. 2005) and the simulations indicate that the degree of unsteadiness is related to the flow type. Unsteadiness is most severe in hydraulic jump flows, where the associated wakes and gap flows (and rotors) display considerable variation over time. Another possibility in three dimensions is interaction between different flow types. This was particularly evident in one simulation where unsteady channelled flow associated with a hydraulic jump imparted acceleration and unsteadiness to the surface winds associated with a neighbouring lee wave field. Meanwhile the winds were still modulated in space by the lee waves themselves.

A special case involving an upstream inversion at a height below the peak height of the orography was simulated. This is not represented in the the regime diagram, though inversions of this kind clearly do occur (see Mobbs et al. 2005). Hydraulic jumps become much more likely for this profile. A hydraulic jump occurs even though the value of the upstream Froude number, $F_i = 1.0$, is twice the maximum Froude number for a hydraulic jump in the regime diagram for mountain heights less than the inversion height.

In addition to validating the regime diagram, the simulations carried out give an insight into the dynamics of the flows. Such knowledge is desirable in order to improve forecasts of the conditions associated with rotors. The dynamic behaviour of the flows is to be explored in a further paper (Sheridan & Vosper 2005).

References

Allen, T. & Brown, A. R. (2002) Large-eddy simulation of turbulent separated flow over rough hills. *Bound.-Lay. Meteorol.* **102**: 177–198.

Baines, P. G. (1995) *Topographic Effects in Stratified Flow.* Cambridge: Cambridge University Press, 482 pp.

Doyle, J. D. & Durran, D. R. (2002) The dynamics of mountain-wave-induced rotors. *J. Atmos. Sci.* **59**: 186–201.

Gal-Chen, T. & Somerville, R. (1975) On the use of a coordinate transformation for the solution of the Navier–Stokes equations. *J. Comp. Phys.* **17**: 209–228.

Mobbs, S. D., Vosper, S. B., Sheridan, P. F., Cardoso, R., Burton, R. R., Arnold, S. J., Hill, M. K., Horlacher, V. & Gadian, A. M. (2005) Observations of downslope winds and rotors in the Falkland Islands. *Q. J. R. Meteorol. Soc.* **131**: 329–351.

Sheridan, P. F. & Vosper, S. B. (2005) Numerical simulations of rotors, hydraulic jumps and eddy shedding in the Falkland Islands. *Atmos. Sci. Lett*. In press.

Vosper, S. B. (2003) Development and testing of a high resolution mountain-wave forecasting system. *Meteorol. Appl*. **10**: 75–86.

Vosper, S. B. (2004) Inversion effects on mountain lee waves. *Q. J. R. Meteorol. Soc*. **130**: 1723–1748.

Wood, N. & Mason, P. J. (1993) The pressure force induced by neutral, turbulent flow over hills. *Q. J. R. Meteorol. Soc*. **119**: 1233–1267.

Wood, N. (1995) The onset of separation in neutral, turbulent flow over hills. *Bound.-Lay. Meteorol*. **76**: 137–164.